Uncertainty of the beam energy measurement in the e^+e^- collision using Compton backscattering*

MO Xiao-Hu(莫晓虎)[1)]

Institute of High Energy Physics, Chinese Academy of Sciences, Beijing 100049, China

Abstract: The beam energy is measured in the e^+e^- collision by using Compton backscattering. The uncertainty of this measurement process is studied by virtue of analytical formulas, and the special effects of variant energy spread and energy drift on the systematic uncertainty estimation are also studied with the Monte Carlo sampling technique. These quantitative conclusions are especially important for understanding the uncertainty of the beam energy measurement system.

Key words: Compton backscattering, uncertainty, energy shift

PACS: 32.80.Aa, 06.20.Dk, 29.30.Kv **DOI:** 10.1088/1674-1137/38/10/106203

1 Introduction

The upgraded Beijing electron-positron collider (BEPCⅡ) is a τ-charm factory with a center mass of energy ranging from 2.0 to 4.6 GeV and a design peak luminosity of 10^{33} $cm^{-2}s^{-1}$ at a beam energy of 1.89 GeV [1, 2]. The upgraded Beijing spectrometer detector (BESⅢ) with high efficiency and good resolution for both charged and neutral particles was constructed and started data taking in 2008 [3]. The BESⅢ research region covers charm physics, charmonium physics, the spectroscopy of light hadrons and τ-lepton physics [4].

After vast amounts of data are acquired and analyzed, the statistical uncertainties in analyses of physics become smaller and smaller, while the systematic uncertainties play more and more prominent roles [5–7], one of which is the uncertainty due to the measurement of beam energy. To reduce such an uncertainty, starting from 2007, a high accuracy beam energy measurement system (BEMS) was designed, constructed, and put into operation at the end of 2010 [8–11], which is of great importance for many physics analyses at BESⅢ, such as τ mass measurement, charmonium resonance scans, and the determination of the branching ratio with the uncertainty at a level of 1% to 2%. The measurement procedure of BEMS can be recapitulated as follows [12]: firstly, the laser source provides the laser beam and the optics system focuses the laser beam and guides it to make head-on collisions with the electron (or positron) beam in the vacuum pipe, after that the backscattering high energy photon will be detected by the High Purity Germanium (HPGe) detector, which is the key instrument of BEMS. The accuracy of beam energy depends merely on the detection result of the backscattering photon.

The essence of the working principle of BEMS is the Compton backscattering process (CBS). In order to understand the main feature of BEMS, the uncertainty of this measurement process is addressed by virtue of analytical formulas, where some experimentally meticulous details are neglected. These acquired quantitative results are of greatest consequence for the qualitatively understanding the actual uncertainty of BEMS. Moreover, an experimentally special phenomenon is studied by the simulation approach, which reveals a possible source of systematic uncertainty of BEMS.

2 Energy formulas

Considered here is a special and crucial case of CBS, that is the electron makes a head-on collision with the photon, whose geometry is sketched in Fig. 1. The energies of the electron and photon before (denoted by subscript 1) and after (denoted by subscript 2) and the collisions are denoted as $\varepsilon_{1,2}$ (for electron) and $\omega_{1,2}$ (for photon), respectively.

In light of the special theory of relativity, the energy and momentum can be expressed as

$$\omega=h\nu\ , \quad p_\gamma=\frac{\omega}{c}\ , \tag{1}$$

Received 17 December 2013

∗ Supported by National Natural Science Foundation of China (NSFC) (11375206, 10775142, 10825524, 11125525, 11235011)

1) E-mail: moxh@mail.ihep.ac.cn

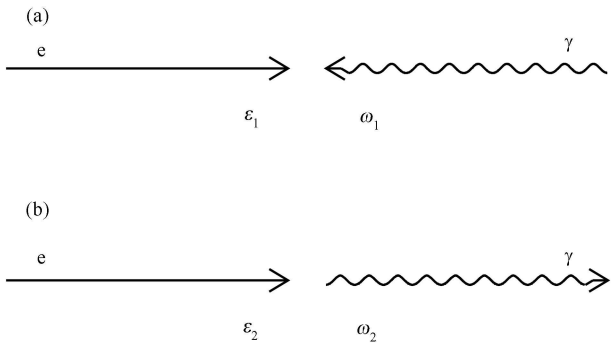

Fig. 1. Geometry of electron (e) and photon (γ) before (a) and after (b) the head-on collision. The stright line denotes e while the wavy line γ.

for the photon and

$$\varepsilon=\frac{m_{\rm e}c^2}{\sqrt{1-\dfrac{v^2}{c^2}}}\ , \quad p_{\rm e}=\frac{\varepsilon v}{c^2}, \tag{2}$$

for the electron. In the above equations, h is the Plant constant and $m_{\rm e}$ is the electron mass. With Eqs. (1) and (2), it is readily able to obtain the kinematic for the electron and photon collision systems. According to the law of energy and momentum conservation,

$$\omega_1+\varepsilon_1=\omega_2+\varepsilon_2, \tag{3}$$

and

$$-\frac{\omega_1}{c}+\frac{\varepsilon_1 v_1}{c^2}=\frac{\omega_2}{c}+\frac{\varepsilon_2 v_2}{c^2},$$

or

$$-\omega_1+\frac{\varepsilon_1 v_1}{c}=\omega_2+\frac{\varepsilon_2 v_2}{c}. \tag{4}$$

Based on the Eqs. (3) and (4), it can be obtained with simple algebra

$$\omega_2=\frac{\varepsilon_1^2\left(1+\dfrac{v_1}{c}\right)^2}{2\varepsilon_1\left(1+\dfrac{v_1}{c}\right)+\dfrac{m_{\rm e}^2c^4}{\omega_1}}. \tag{5}$$

For BESIII, the optimal energy point is at 1.89 GeV, the velocity of electron with such a high energy is very close to that of light (c), in other words, $v_1/c\approx 1$ with the negligible error. With such an approximation, Eq. (5) is recast as

$$\omega_2=\frac{\varepsilon_1^2}{\varepsilon_1+\dfrac{m_{\rm e}^2c^4}{4\ \omega_1}}. \tag{6}$$

In BEMS, ω_1 is provided by the laser and ω_2 is measured by the HPGe detector, and ε_1 is the beam energy that is to be determined with high accuracy. From Eq. (5), it is worked out

$$\varepsilon_1=\frac{\omega_2}{2}\left(1+\sqrt{1+\frac{m_{\rm e}^2\ c^4}{\omega_1\ \omega_2}}\right)+\frac{m_{\rm e}^2}{2\omega_2\left(1+\sqrt{1+\dfrac{m_{\rm e}^2\ c^4}{\omega_1\ \omega_2}}\right)}, \tag{7}$$

or from Eq. (6), it is acquired

$$\varepsilon_1=\frac{\omega_2}{2}\left(1+\sqrt{1+\frac{m_{\rm e}^2\ c^4}{\omega_1\ \omega_2}}\right). \tag{8}$$

3 Uncertainty formulas

The starting point of the uncertainty analysis of this section is the two formulas obtained in the previous section, viz. Eqs. (7) and (8). For brevity, in this section we adopt the nature unity where $c=1$ (the subscript e is also suppressed for electron mass) and begin with the comparatively simple case, that is Eq. (8), by virtue of which it is immediately obtained

$$\begin{aligned}
\frac{\partial\varepsilon_1}{\partial m} &= \frac{m}{2\omega_1}\cdot\frac{1}{\sqrt{1+\dfrac{m^2}{\omega_1\omega_2}}},\\
\frac{\partial\varepsilon_1}{\partial\omega_1} &= -\frac{m^2}{4\omega_1^2}\cdot\frac{1}{\sqrt{1+\dfrac{m^2}{\omega_1\omega_2}}},\\
\frac{\partial\varepsilon_1}{\partial\omega_2} &= \frac{1}{2}\left(1+\sqrt{1+\frac{m^2}{\omega_1\omega_2}}\right)-\frac{m^2}{4\omega_1\omega_2}\cdot\frac{1}{\sqrt{1+\dfrac{m^2}{\omega_1\omega_2}}}.
\end{aligned} \tag{9}$$

On the strength of Eq. (8), Eq. (9) can be rewritten in a more concise forms as follows

$$\begin{aligned}
\frac{\partial\varepsilon_1}{\partial m} &= \frac{\varepsilon_1}{m}\left(1-\frac{1}{\sqrt{1+\dfrac{m^2}{\omega_1\omega_2}}}\right),\\
\frac{\partial\varepsilon_1}{\partial\omega_1} &= -\frac{\varepsilon_1}{2\omega_1}\left(1-\frac{1}{\sqrt{1+\dfrac{m^2}{\omega_1\omega_2}}}\right),\\
\frac{\partial\varepsilon_1}{\partial\omega_2} &= \frac{\varepsilon_1}{2\omega_2}\left(1+\frac{1}{\sqrt{1+\dfrac{m^2}{\omega_1\omega_2}}}\right).
\end{aligned} \tag{10}$$

The compact expression for the uncertainty evaluation is as follows:

$$\frac{\delta\varepsilon_1}{\varepsilon_1}=\frac{f_+}{2}\cdot\frac{\delta\omega_2}{\omega_2}\oplus\frac{f_-}{2}\cdot\frac{\delta\omega_1}{\omega_1}\oplus f_-\cdot\frac{\delta m}{m}, \tag{11}$$

with factors $f_\pm$ defined as

$$f_\pm=1\pm\frac{1}{\sqrt{1+\dfrac{m^2}{\omega_1\omega_2}}}. \tag{12}$$

Now we turn to Eq. (7). A similar process as that for Eq. (8) could lead to fairly cumbersome derivative expressions of ε_1 with respect to ω_2, ω_1, or m, which have been degraded into appendix A. Herein we present another recipe. Comparing Eqs. (7) and (8), it is clear that Eq. (8) is just the first term of Eq. (7), therefore it is natural to find an uncertainty expression for Eq. (7) which could incorporate the result acquired based on Eq. (8). To this end, we return to Eq. (5). If a function of ε_1, $g(\varepsilon_1)$, is introduced, Eq. (5) becomes

$$\omega_2=\frac{g^2(\varepsilon_1)}{2g(\varepsilon_1)+\dfrac{m^2}{\omega_1}}. \tag{13}$$

with

$$g(\varepsilon_1)=\varepsilon_1\left(1+\frac{v_1}{c}\right)=\varepsilon_1+\sqrt{\varepsilon_1^2-m^2}. \tag{14}$$

Then it is readily obtained by

$$g(\varepsilon_1)=\omega_2\cdot\left(1+\sqrt{1+\frac{m^2}{\omega_1\ \omega_2}}\right), \tag{15}$$

and

$$\varepsilon_1=\frac{g}{2}+\frac{m^2}{2g}. \tag{16}$$

Noticing the similarity between Eqs. (8) and (15), it is immediately obtained

$$\frac{\delta g}{g}=\frac{f_+}{2}\cdot\frac{\delta\omega_2}{\omega_2}\oplus\frac{f_-}{2}\cdot\frac{\delta\omega_1}{\omega_1}\oplus f_-\cdot\frac{\delta m}{m}. \tag{17}$$

Next, from Eq. (16), it also easy to get

$$\frac{\delta\varepsilon_1}{\varepsilon_1}=\frac{g^2-m^2}{g^2+m^2}\cdot\frac{\delta g}{g}\oplus\frac{2m^2}{g^2+m^2}\cdot\frac{\delta m}{m}. \tag{18}$$

4 Statistical and systematic uncertainties

Analytical formulas acquired in the previous section are the foundation for the uncertainty analysis relevant to CBS. In principle, there are two types of uncertainty: statistical and systematic. In a nutshell, the statistical are those types of uncertainties that have a random spread, and their uncertainties decrease with augment of data; the systematic includes everything else. In practice, it is not always easy to distinguish two types of uncertainty, and sometimes it is rather difficult to identify the feature of systematic uncertainty. For example, as to each term in the error formulas such as Eqs. (11) and (18), it could include both statistical and systematic uncertainties. From a pragmatistic point of view, we lay stress on the relative magnitude of each term instead of focusing on its feature, and try to figure out the leading contribution for the uncertainty evaluation.

Table 1. Some parameters related to BCS.

parameter	central value (value scope)	relative error	reference
m_e	0.51099828 MeV	2.153×10^{-8}	[13]
ω_1	0.114426901 eV	8.739×10^{-9}	[10, 14]
ω_2	(2–7) MeV	5×10^{-5}	[10, 12]

To begin with, we estimate the deviation from 1 for the factor $f_\pm$ defined in Eq. (12). With m_e = 0.51099828 MeV, $\omega_1 = 0.114426901$ eV, and ω_2 ranges from 2 to 7 MeV, the corresponding deviation is within the scope $\pm$(0.94–1.75)‰. Therefore, it is accurate enough to approximate $f_\pm$ as 1. Then, according to the values listed in Table 1, the relative errors of m_e and ω_1 are three orders of magnitude lower than that of ω_2, which means the leading contribution for the uncertainty of BCS is the first term in Eq. (11), that is to say we have the relation

$$\frac{\delta\varepsilon_1}{\varepsilon_1}\approx\frac{1}{2}\frac{\delta\omega_2}{\omega_2}, \tag{19}$$

with fairly high accuracy (the additional uncertainty is much less than 10^{-3}).

Equation (19) indicates that the feature of the electron (positron) beam (denoted by ε_1 and $\delta\varepsilon_1$) is totally determined by that of the backscattering photon (denoted by ω_2 and $\delta\omega_2$), and vice versa. With the use of BEMS, ω_2 is determined by the position of the Compton edge while $\delta\omega_2$ by the slope of the edge[1)]. Herein, the existent of an edge slope is just due to $\delta\varepsilon_1$, the energy spread of accelerator. It is noticeable en passant that ε_1 and $\delta\varepsilon_1$ are constants during measurement. For the certain beam energy (fixed ε_1), the energy spread ($\delta\varepsilon_1$) is solely determined by the structure of the accelerator itself and therefore must be fixed in common sense [15]. However, during the data taking of the J/ψ sample performed in 2012, a peculiar phenomenon is found. As shown in Fig. 2, it is noticed that the cross sections vary with the decrease of beam current, which means there are some variations of beam status during energy measurement[2)]. Such variations imply the variant energy, or energy spread, or both of them. The effects, as being elucidated in the next section, can lead to an energy shift in the measurement of beam energy. This is a crux matter for the uncertainty analysis of BEMS.

1) The details of measurement of ω_2 and $\delta\omega_2$ are delineated in the next section.

2) For BEPC Ⅱ, in order to control the fluctuation of beam current, a feedback system is added which may affect the stability of energy spread. This means the energy spread may change for the fixed beam energy.

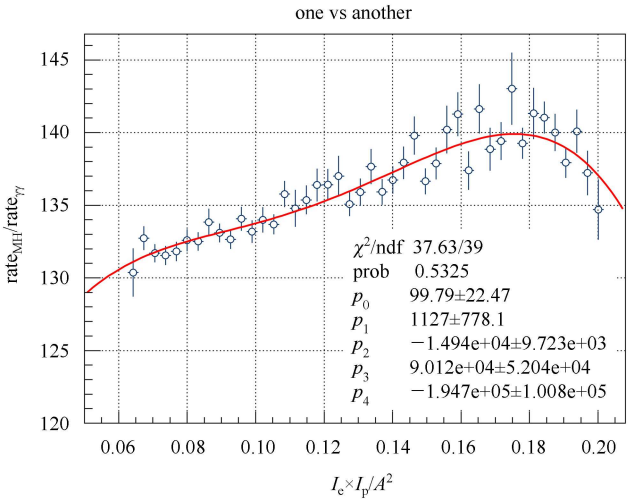

Fig. 2. The relation between beam current and the "relative" cross section with data taken at J/ψ resonance. The horizontal scale is denoted by "$I_e\times I_p/A^2$ " which means the product of the electron current (I_e) and the positron current (I_p), whose unit is the square of Ampere. The ratio of the number of inclusive hadronic events to that of the two-gamma events (both from online database), which is proportional to the observed cross section, is denoted as "relative" cross section.

5 Effects of variations of energy spread and energy drift on measured energy

This section is devoted to the investigation of effects of variations of energy spread and drift on measured energy. Two cases are considered: 1) assuming there is no energy drift, the energy shift is only due to the variation of energy spread; 2) assuming energy spread is fixed, the energy shift is only due to the energy drift. The Monte Carlo simulation approach is adopted for the following study.

5.1 Simulation of Compton edge

The backscattering photons from a head-on collision with the electron (positron) beam will form a sharp edge in a detective spectrum. The pure sharp edge at certain energy (denoted by ω) is approximated by the normalized function [16]

$$h(x)=[p_3+p_2(x-p_0)]\Theta(p_0-x). \quad (20)$$

Here, the product $p_2(x-p_0)$ is small compared to p_3; for $p_2=0$ and $p_3=1$, $h(x)$ reduces to the normal step function. The function $h(x)$ is then folded with a Gaussian of standard deviation

$$g(x)=\frac{1}{\sqrt{2\pi}p_1}\mathrm{e}^{-\frac{x^2}{2p_1^2}}. \quad (21)$$

The resulting function for the variable position and height of the edge is given by

$$f(x)=\int_{-\infty}^{+\infty}\mathrm{d}t\ h(t)g(x-t). \quad (22)$$

Anyway, due to the existence of a background, a linear function $p_4(x-p_0)+p_5$ is added to $f(x)$ to describe the shape of the background. Therefore, the final synthetic function has the form:

$$g(x,\vec{p}) = \frac{1}{2}(p_2(x-p_0)+p_3)\cdot\mathrm{erfc}\left[\frac{x-p_0}{\sqrt{2}p_1}\right] - \frac{p_1p_2}{\sqrt{2\pi}}\cdot\exp\left[-\frac{(x-p_0)^2}{2p_1^2}\right]+p_4(x-p_0)+p_5, \quad (23)$$

with [17]

$$\mathrm{erfc}(z)\equiv\frac{2}{\sqrt{\pi}}\int_z^\infty \mathrm{d}u\ \mathrm{e}^{-u^2}.$$

The parameters in Eq. (23) are: p_0-edge position; p_1-edge width; p_2-slope left; p_3-edge amplitude; p_4-slope right; p_5-background. Parameter p_0 gives the information about the average electron beam energy during the data acquisition period, while p_1 is mostly coupled with the electron beam energy spread.

In the simulation, the following form is adopted

$$f(x) = \frac{1}{2}a_2[q+a_1(x-\omega)]\cdot\mathrm{erfc}\left[\frac{x-\omega}{\sqrt{2}\sigma}\right] - \frac{qa_1a_2}{\sqrt{2\pi}}\cdot\exp\left[-\left(\frac{x-\omega}{\sqrt{2}\sigma}\right)^2\right]+b_2[q+b_1(x-\omega)], \quad (24)$$

where ω is the position of the Compton edge that is used to determine the beam energy; σ is the edge width that is related with the beam energy spread (σ_s); q is the unity parameter that is used to determine the unity of x ($q=1$, the unity of x is MeV while $q=1000$, the unity of x is keV).

Table 2. Input parameters for Compton edge simulation.

parameter	value
m_e/MeV	0.51099828
ω_0/eV	0.114426901
E_{cm}/MeV	3096.916
Δ/MeV	1
ϵ/MeV	1548.418
σ_s/MeV	0.707107
ω/keV	4190.521
σ/keV	3.8272
q	1000
a_1	−0.1
a_2	0.3
b_1	−0.2
b_2	0.1

The relation between ω and ϵ is as follows[1)]

$$\omega=\frac{\epsilon^2}{\epsilon+\dfrac{m_{\rm e}^2}{4\ \omega_0}},\quad \epsilon=\frac{\omega}{2}\left(1+\sqrt{1+\frac{m_{\rm e}^2}{\omega\omega_0}}\right);$$

and the relation between $\sigma_{\rm s}$ and σ is as follows[2)]

$$\sigma=2\cdot\frac{\omega}{\epsilon}\cdot\sigma_{\rm s}.$$

In addition, it should be noted that $\epsilon=E_{\rm cm}/2$ and $\sigma_{\rm s}=\Delta/\sqrt{2}$, where $E_{\rm cm}$ is the center-of-mass (C.M.) energy, and Δ is the spread of $E_{\rm cm}$. For the energy at J/ψ resonance, the input parameters for the Compton edge simulation are tabulated in Table 2.

5.2 Relation between the observed cross section and energy spread

The cross section of the process $\rm e^+e^-\to J/\psi\to f$ (where f denotes some final state) is described by the Breit-Wigner formula

$$\sigma_{\rm BW}(s)=\frac{12\pi\cdot\Gamma_{\rm e}\Gamma_{\rm f}}{(s-M^2)^2+\Gamma_{\rm t}^2M^2},\tag{25}$$

where $\sqrt{s}$ is the C.M. energy ($\sqrt{s}=E_{\rm cm}$), $\Gamma_{\rm e}$ and $\Gamma_{\rm f}$ are the widths of J/ψ decaying into $\rm e^+e^-$ and f, Γ_t and M are the total width and mass of J/ψ. Taking the initial state radiative correction into consideration, the cross section becomes [18]

$$\sigma_{\rm r.c.}(W)=\int_0^{x_{\rm m}}{\rm d}xF(x,s)\frac{1}{|1-\Pi(s(1-x))|^2}\sigma_{\rm BW}(s(1-x)),\tag{26}$$

where $x_m=1-s'/s$, $\sqrt{s'}$ is the experimentally required minimum invariant mass of the final state f after losing energy due to multi-photon emission; $F(x,s)$ has been calculated in many references [18–20] and $\Pi(s(1-x))$ is the vacuum polarization factor. The $\rm e^+e^-$ colliders have finite energy spread. The energy spread function $G(\sqrt{s},\sqrt{s'})$ is usually a Gaussian distribution:

$$G(\sqrt{s},\sqrt{s'})=\frac{1}{\sqrt{2\pi}\Delta}{\rm e}^{-\frac{(\sqrt{s}-\sqrt{s'})^2}{2\Delta^2}},\tag{27}$$

where Δ describes the C.M. energy spread of the accelerator, $\sqrt{s}$ and $\sqrt{s'}$ are the nominal and actual C. M. energy respectively. So the experimentally measured resonance cross section (observed cross section) is the radiatively corrected Breit-Wigner cross section folded with the energy spread function:

$$\sigma_{\rm exp}(\sqrt{s})=\int_0^{\infty}\sigma_{\rm r.c.}(\sqrt{s'})G(\sqrt{s'},\sqrt{s}){\rm d}\sqrt{s'},\tag{28}$$

where $\sigma_{\rm r.c.}$ is defined by Eq. (26).

The numerical calculation indicates that the radiative correction reduces the maximum cross section of J/ψ by 52%; the energy spread further lowers down the cross section by an order of magnitude depending on the value of the energy spread. Both the radiative correction and the energy spread shifts the maximum height of the resonance peak to above the resonance nominal mass. In actual experiments, data are naturally taken at the energy which yields the maximum inclusive hadron cross section. When the energy spread changes, both the maximum cross section and the position of energy for the maximum cross section change correspondingly.

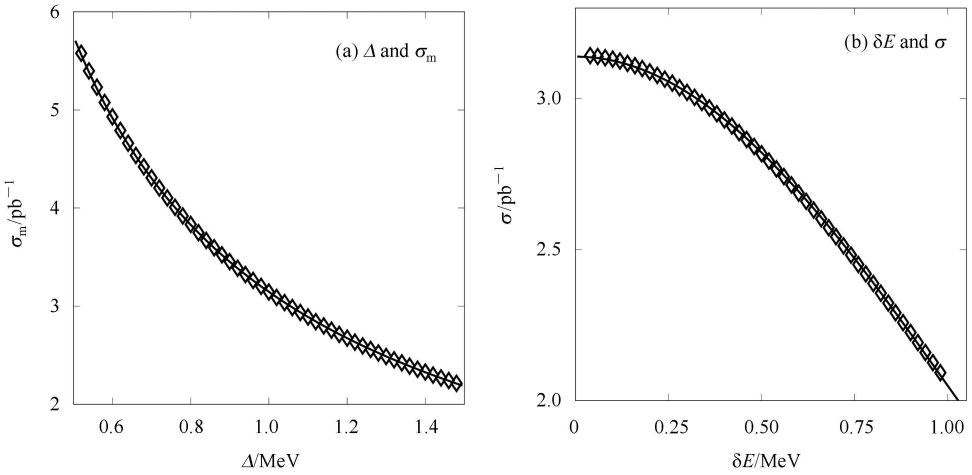

Fig. 3. The relation between the energy spread Δ and the maximum observed cross section $\sigma_{\rm m}$ (a), and the energy shift δE and the observed cross section σ (b).

1) The relation is just Eqs. (6) and (8), with the correspondence $\omega=\omega_2$, $\epsilon=\varepsilon_1$, $\omega_0=\omega_1$ and $\omega=\omega_2$.
2) The relation is just Eq. (19), with the correspondence $\epsilon=\varepsilon_1$, $\sigma_{\rm s}=\delta\varepsilon_1$, $\omega=\omega_2$ and $\sigma=\delta\omega_2$.

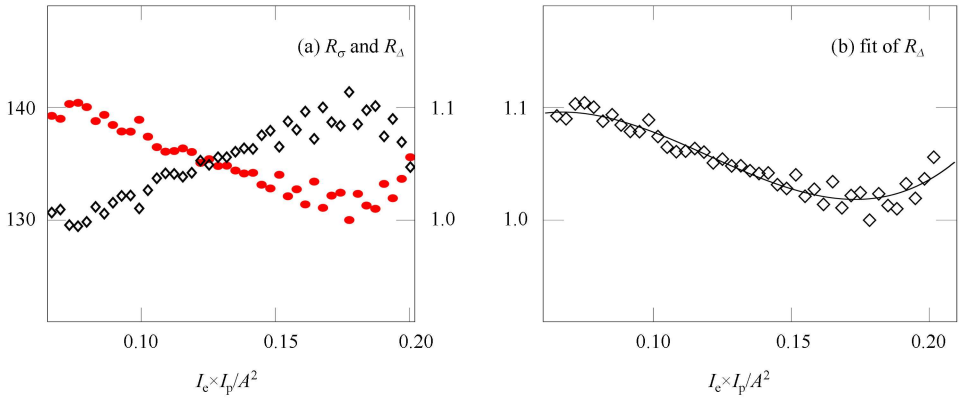

Fig. 4. The relation between beam current and the "relative" cross section, R_σ (denoted by diamond in (a)) and "relative" energy spread R_Δ (denoted by solid circle in (a)). The horizontal scale is denoted by "$I_e \times I_p/A^2$" which means the product of electron current (I_e) and positron current (I_p), whose unit is the square of Ampere.

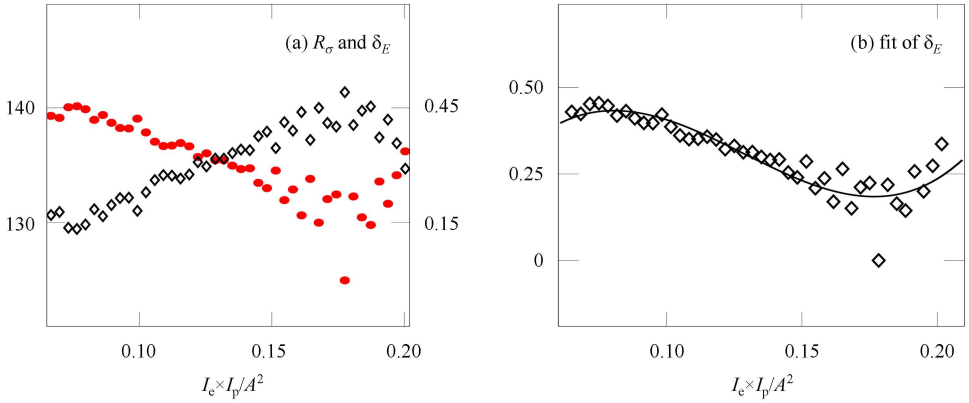

Fig. 5. The relation between beam current and the "relative" cross section, R_σ (denoted by diamond in (a)) and energy drift δ_E (denoted by solid circle in (a)). The horizontal scale is denoted by "$I_e \times I_p/A^2$" which means the product of the electron current (I_e) and positron current (I_p), whose unit is the square of Ampere.

5.3 Relation of the cross section with energy spread and energy drift

The minimization subroutine program DMINFC from CERNLIB [21] is used to find the position of energy ($E_{\rm max}$) for the maximum cross section and the corresponding maximum cross section ($\sigma_{\rm m}$) itself corresponding to distinctive energy spread (Δ). The energy shift ($\delta E_{\rm mn}$) is defined as the difference between the maximum energy ($E_{\rm max}$) and the nominal energy ($E_{\rm nom}$=3096.916 MeV), that is

$$\delta E_{\rm mn}=E_{\rm max}-E_{\rm nom},$$

and the fit curve for $\delta E_{\rm mn}$ against Δ is

$$f_{\delta E_{\rm mn}}(x)[{\rm keV}]=1.1117\cdot x[{\rm MeV}]+98.567, \quad (29)$$

and the fit curve for $\sigma_{\rm m}$ against Δ is (refer to Fig. 3(a))

$$f_{\sigma_{\rm m}}(x)[{\rm pb}^{-1}]=3.3885/x^{0.82322}-0.24237, \quad [x\text{: MeV}]. \quad (30)$$

In Fig. 4(a), the ordinate is the ratio of the number of inclusive hadronic events to that of the two-gamma events, which is proportional to the observed cross section and denoted as the "relative" cross section (R_σ) in this monograph; in Fig. 4(b), the ordinate is the ratio of the two energy spread, denoted as the "relative" energy spread (R_Δ). The fit curve for R_Δ against $I_e \times I_p$ is

$$f_{R_\Delta}(x)=0.96451+4.5012\cdot x-46.612\cdot x^2+129.44\cdot x^3. \quad (31)$$

Figure 3(b) shows the relation between the observed cross section σ and energy drift δ_E, which is defined as follows

$$\delta_E=E-E_{\rm max},$$

where $E_{\rm max}=3096.9981$ MeV corresponding to the energy spread 1 MeV. The fit curve is

$$f_\sigma(x)[{\rm pb}^{-1}]=3.1391\cdot {\rm e}^{-0.42638\cdot x^2}, \quad [x\text{: MeV}]. \quad (32)$$

The ordinate of Fig. 5(a) is the same as that of Fig. 4(a); the ordinate of Fig. 5(b) is the energy drift, denoted as δ_E. The fit curve for δ_E against $I_e \times I_p$ is

$$f_{\delta_E}(x)=-0.38548+23.955\cdot x-216.47\cdot x^2+561.15\cdot x^3. \quad (33)$$

As a matter of fact, in order to obtain the relation between R_σ and R_Δ (δ_E), the special normalization is adopted. The nitty-gritty is elaborated in appendix B. Here, $f_{R_\Delta}(x)$ in Eq. (31) and $f_{\delta_E}(x)$ in Eq. (33) reflect the possible variations of energy spread or energy drift within one beam injection, and can be treated as a probability function for the variation of R_Δ and δ_E. Therefore, the variable x should take the value between 0 and 1. In the following simulation, the acceptance-rejection technique [22, 23] is adopted for distribution sampling.

5.4 Fitted energy for different cases

5.4.1 Effect due to variant energy spread

The simulation for the Compton edge is performed for two cases: 1) for the fix energy spread, the sampling of the edge is according to distribution formulated in Eq. (24); 2) for the variate energy spread, the sampling of the edge is also according to the distribution formulated in Eq. (24) but with variate σ, that is the fix value of σ is replaced by variant $\sigma(x)$, i.e.

$$\sigma(x)=\sigma\cdot f_{R_\Delta}(x),$$

where $f_{R_\Delta}(x)$ is the distribution in Eq. (31), and x is a random number in between 0 and 1. The simulated distributions for two cases are shown in Fig. 6(a).

The fitted results based on the simulated distributions for two cases are given in Table 3, and the fit curves

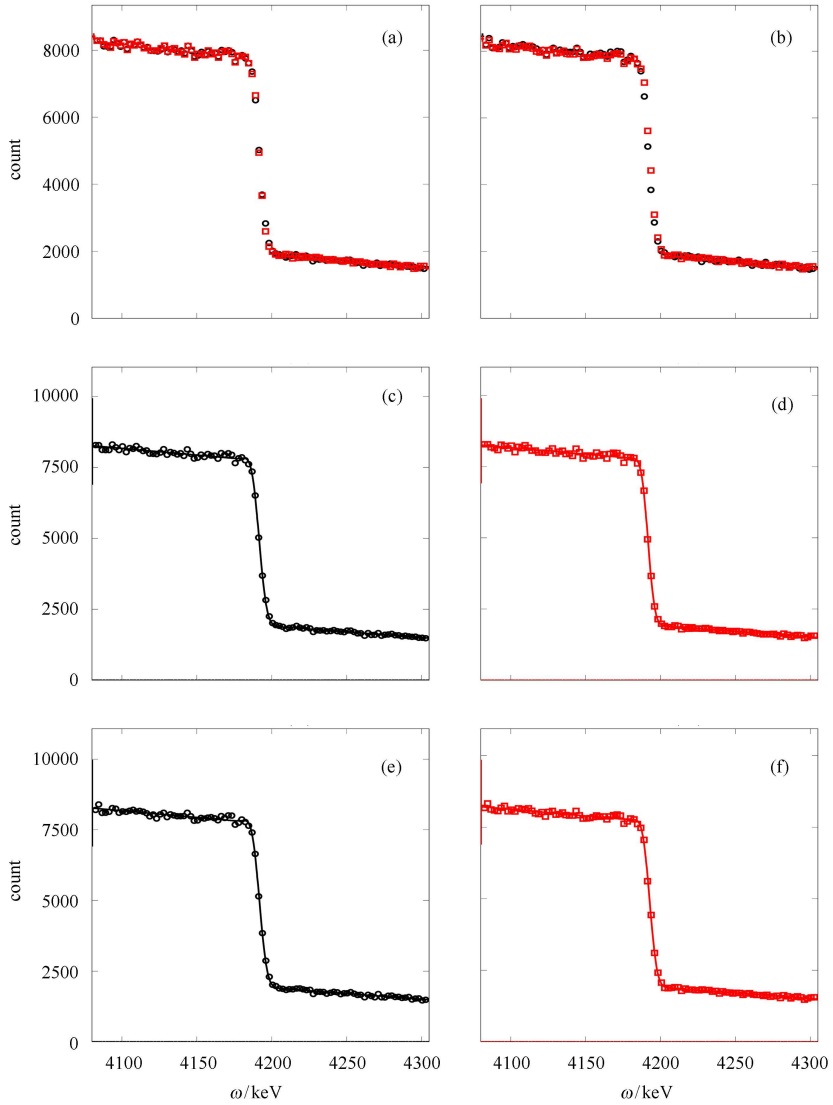

Fig. 6. The comparison of simulations of the Compton edge for different cases: fix and variant energy spread (a); fix and variant energy drift (b). The fit results for different cases: fix energy (c) and variant energy spread (d); fix energy (e), with energy drift (f). Herein, $E_{\rm cm}$ is distinctive for (c) and (d) as indicted in Table 4. The circle plots denote the fix cases while the box plots the variant cases; the curve is the best fit result. There are 0.5 Million counts in each sample.

Table 3. The fit results of beam energy for different cases of energy spread: fix energy spread and variant energy spread.

parameter	fix σ	variant σ
χ^2	83.64406	77.50543
ϵ/MeV	1548.300±0.082	1548.413±0.115
Δ/MeV	1.1215±0.0480	1.0924±0.0573
a_1	−0.12464±0.01937	−0.10374±0.03012
a_2	5.8016±0.0281	5.7938±0.0285
b_1	−2.0528±0.0807	−2.0300±0.0819
b_2	1.9456±0.0134	1.9471±0.0133

Table 4. The fit results of beam energy for different cases of energy drift: fix energy and with energy drift. The input $E_{\rm cm}$=3096.9981 GeV instead of $E_{\rm cm}$=3096.916 GeV.

parameter	fix ω	variant ω
χ^2	86.93219	76.01074
ϵ/MeV	1548.339±0.078	1548.572±0.100
Δ/MeV	1.1211±0.0469	1.0631±0.0517
a_1	−0.12588±0.01884	−0.11371±0.02701
a_2	5.7998±0.0280	5.7678±0.0283
b_1	−2.0572±0.0804	−2.0276±0.0822
b_2	1.9461±0.0134	1.9384±0.0132

for two cases is displayed in Fig. 6(c) and (d). The difference for fitted beam energy is about 0.113 MeV, or 0.226 MeV for C.M. energy.

5.4.2 Effect due to energy drift

The simulation for the Compton edge is performed for two cases: 1) for the fix energy, the sampling of the edge is according to the distribution formulated in Eq. (24); 2) for the variant energy, the sampling of the edge is also according to the distribution formulated in Eq. (24) but with variant ω, the fix value of ω is replaced by variate $\omega(x)$, i.e.

$$\omega(x)=\omega\cdot f_{\delta_E}(x)\ ,$$

where $f_{\delta_E}(x)$ is the distribution in Eq. (33), and x is a random number between 0 and 1. The simulated distributions for the two cases are shown in Fig. 6(b).

The fitted results based on the simulated distributions for two cases are given in Table 4, and the fit curves for the two cases is displayed in Fig. 6(e) and (f). The difference for the fitted beam energy is about 0.233 MeV, or 0.466 MeV for C.M. energy.

6 Summary

In this monograph, the energy relation between the Compton backscattering photon and high energy electron is derived analytically, based on which the formula for an uncertainty estimation of measured energy is obtained. The leading contribution of uncertainty is figured out by utilizing the present experimental information.

By virtue of the experimentally available information, the special phenomenon between the beam current and cross section is explored in detail by the simulation approach. The quantitative results indicate that for C.M. energy, the maximum energy shift is up to 0.226 MeV due to variant energy spread and 0.466 MeV due to variant energy drift. These effects of energy shift studied herein disclose so to speak a significantly possible source of systematic uncertainty for BEMS, which in turn has the far-reaching meaning for the further analysis of the physics error.

Author acknowledges Dr. JianYong Zhang for his providing information on the relation between beam current and cross section.

Appendix A

The nature unity with $c=1$ is adopted hereafter. The velocity of the electron is denoted as $\beta(=v/c)$ and its corresponding energy is often expressed as $\varepsilon=m\gamma$ with $\gamma=1/\sqrt{1-\beta^2}$. According to Refs. [24, 25], the general relation between ω_1 and ω_2 for the Compton scattering process is

$$\omega_2=\frac{\omega_1(1-\beta\cos\phi_1)}{1-\beta\cos\phi_2+\dfrac{\omega_1}{\gamma m}(1-\cos[\phi_1-\phi_2])},\qquad\text{(A1)}$$

where ϕ_1 is the angle between the incident photon and electron while ϕ_2 is the angle between the backscattering photon and electron. For a head-on collison, $\phi_1=180^\circ$ and $\phi_2=0^\circ$, so Eq. (A1) becomes

$$\omega_2=\frac{\omega_1(1+\beta)}{(1-\beta)+\dfrac{2\omega_1}{\gamma m}}=\frac{\dfrac{1+\beta}{1-\beta}}{\dfrac{1}{\omega_1}+\dfrac{2}{m\gamma(1-\beta)}}\ ,\qquad\text{(A2)}$$

Note the two relations

$$\frac{1+\beta}{1-\beta}=\gamma^2(1+\beta)^2,\quad \frac{1}{\gamma(1-\beta)}=\gamma(1+\beta),$$

and also the relation $m^2\gamma^2=\varepsilon_1^2$, Eq. (A2) can be rewritten as

$$\omega_2=\frac{\varepsilon_1^2(1+\beta)^2}{2\varepsilon_1(1+\beta)+\dfrac{m^2}{\omega_1}}\ ,\qquad\text{(A3)}$$

and this is just Eq. (5), from which it yields

$$\varepsilon_1=\frac{\omega_2}{2}\left(1+\sqrt{1+\frac{m^2}{\omega_1\ \omega_2}}\right)+\frac{m^2}{2\omega_2\left(1+\sqrt{1+\dfrac{m^2}{\omega_1\ \omega_2}}\right)}.\qquad\text{(A4)}$$

Then the partial derivative with respect to ω_1, ω_2, and m can be expressed by

$$\begin{aligned}\frac{\partial\varepsilon_1}{\partial m} &= \frac{\varepsilon_1}{m}\cdot\left(1-\frac{1}{\kappa}\right)+\frac{m}{\omega_2}\cdot\frac{1}{\kappa(\kappa+1)},\\ \frac{\partial\varepsilon_1}{\partial\omega_1} &= -\frac{\varepsilon_1}{2\omega_1}\cdot\left(1-\frac{1}{\kappa}\right)+\frac{(\kappa-1)^2}{2\kappa},\\ \frac{\partial\varepsilon_1}{\partial\omega_2} &= \frac{\varepsilon_1}{2\omega_2}\cdot\left(1+\frac{1}{\kappa}\right)-\frac{m^2}{\omega_2^2}\cdot\frac{1}{2\kappa},\end{aligned} \tag{A5}$$

with

$$\kappa\equiv\sqrt{1+\frac{m^2}{\omega_1\omega_2}}\ . \tag{A6}$$

Based on the law of error propagation, the $\delta\varepsilon_1$ is obtained as follows

$$(\delta\varepsilon_1)^2=\left(\frac{\partial\varepsilon_1}{\partial\omega_2}\cdot\delta\omega_2\right)^2\oplus\left(\frac{\partial\varepsilon_1}{\partial\omega_1}\cdot\delta\omega_1\right)^2\oplus\left(\frac{\partial\varepsilon_1}{\partial m}\cdot\delta m\right)^2. \tag{A7}$$

Appendix B

In this appendix, σ, δ and x represent respectively the relative cross section (R_σ), energy spread (R_Δ), and energy drift (δE). Firstly,

$$\begin{aligned}\sigma_1 &= \frac{p_2}{\delta_1^{p_3}}+p_1,\\ \sigma_2 &= \frac{p_2}{\delta_2^{p_3}}+p_1.\end{aligned} \tag{B1}$$

Some algebra yields

$$\frac{1}{r}=\frac{p_2+a_1}{p_2+ka_1}\cdot k,$$

with definitions

$$r=\frac{\sigma_2}{\sigma_1},\quad k=\frac{a_2}{a_1},\quad a_i=p_1\cdot\delta_i^{p_3}\quad (i=1,2).$$

Then it is easy to acquire

$$k=\frac{p_2}{(p_2+a_1)r-a_1}. \tag{B2}$$

With the above relation, if σ_1 and δ_1 (equivalently a_1) are chosen, δ_2 can be calculated from σ_2. In our study, σ_1 is chosen as the maximum cross section, which guarantees k is always greater than 1. As for δ_1, 0.8 MeV, 1.0 MeV, and 1.2 MeV, are used to calculate the σ_2, the shape of curves are exactly the same. Without the loss of generality and actuality, δ_1 is set to be 1.0 MeV.

Secondly, we consider the relation between σ and x.

$$\begin{aligned}\sigma_1 &= p_1\cdot\mathrm{e}^{-p_2\cdot x_1^2},\\ \sigma_2 &= p_1\cdot\mathrm{e}^{-p_2\cdot x_2^2}.\end{aligned} \tag{B3}$$

Some algebra yields

$$\frac{\kappa}{p_2}=\eta(\eta+2x_1),$$

with definitions

$$\kappa=\ln\frac{\sigma_1}{\sigma_2}\ ,\quad \eta=x_2-x_1\ .$$

According to the root formula for the quadratic equation and notice $\eta>0$, then

$$x_2=\sqrt{x_1^2+\kappa/p_2}. \tag{B4}$$

Let x_1 correspond to σ_1 and σ_1 to the maximum cross section, that is $x_1=0$ and $\sigma_1=\sigma_{\max}$, then we have

$$x_2=\sqrt{\frac{1}{p_2}\cdot\ln\frac{\sigma_{\max}}{\sigma_2}}. \tag{B5}$$

References

1 WANG J Q et al. Proceedings of IPAC'10. Kyoto, Japan, 2010. 2359
2 Preliminary Design Report of Accelerator BEPC/, Second version, 2003 (in Chinese). Refer to http://acc- center.ihep.ac.cn/bepcii/bepcii.htm
3 ABLIKIM M et al. Nucl. Instrum. Methods A, 2010, **614**: 345
4 CHAO Kuang-Ta, WANG YI-FANG. Internation Journal of Modern Physics A (Suppl. Issue 1), 2009, **24**: 1
5 FU Cheng-Dong, MO Xiao-Hu. Chinese Physics C (HEP & NP), 2008, **32**: 776
6 MO Xiao-Hu. Nucl. Phys. B (Proc. Suppl.), 2007, **169**: 132
7 WANG You-Kai, MO Xiao-Hu, YUAN Chang-Zheng et al. Nucl. Instrum. Methods A, 2007, **583**: 479
8 Achasov M N et al. Nucl. Phys. B (Proc. Suppl.), 2009, **189**: 366–370
9 MO Xiao-Hu et al. Chinese Physics C (HEP & NP), 2010, **34**: 912–917
10 Abakumova E V et al. Nucl. Instrum. Methods A, 2011, **659**: 21
11 ZHANG J Y et al. Nuclear Physics B, 2012, **225–227**: 309–314
12 MO Xiao-Hu et al. Chinese Physics C (HEP & NP) , 2008, **32**: 995
13 Beringeer J et al. (Particle Data Group). Phys. Rev. D, 2012, **86**: 010001
14 Patkl C K N. Physical Review, 1964, **136**: 1187
15 Lee S Y. Accelerator Physics (2nd Edition). World Scientific Publishing Co. Pte. Ltd., 2004
16 Klein R et al. Nucl. Instrum. Methods A, 1997, **384**: 293
17 Gradshteyn I S, Ryzhik I M. Table of Integrals, Series, and Products. Elsevier Inc., 2007
18 Kuraev E A, Fadin V S. Sov. J. Nucl. Phys., 1985, **41**: 466–472
19 Altarelli G, Martinelli G. CERN, 1986, **86-02**: 47; Nicrosini O, Trentadue L. Phys. Lett. B, 1987, **196**: 551
20 Berends F A, Burgers G, Neerven W L. Nucl. Phys. B, 1988, **297**: 429; Nucl. Phys. B, 1988, **304**: 921
21 CERNLIB - CERN Program Library Short Writeups. CERN Geneva, Switzerland. 1996
22 Brandt S. Data Analysis, Springer-Verlag New York Inc. 1998
23 ZHU Yong-Sheng. Probability and Statistics in Experimental Physics. Second Edition. Scientific Publishing. 2006
24 Rullhusen P, Artru X, Dhez P. Novel Radiation Sources Using Relativistic Electrons. World Scientific Publishing. 1998
25 Landau L D, Lifshitz E M. Relativistic Quantum Mechanics. Pergamon. 1971